Available online at www.sciencedirect.com
ScienceDirect
Trans. Nonferrous Met. Soc. China 24(2014) 3285−3292
Transactions of Nonferrous Metals Society of China
www.tnmsc.cn

Upper bound analysis for hybrid sheet metals extrusion process through curved dies

H. HAGHIGHAT, H. SHAYESTEH
Mechanical Engineering Department, Razi University, Kermanshah 67149−67346, Iran

Received 24 November 2013; accepted 9 March 2014

Abstract: The extrusion process of hybrid sheet metals through arbitrarily curved dies was analyzed by the method of upper bound. The material under deformation was divided into two deformation regions, bimetal and mono-metal regions, and the flow of the material in each region was assumed as plane strain state. The internal, shearing and frictional power terms were derived and they were used in the upper bound model. The extrusion forces for two types of die shapes, an optimum wedge shaped die and an optimum streamlined die shape for a hybrid sheet composed of copper as sleeve and aluminum as core were determined. The corresponding results for those two die shapes were also determined by using the finite element code, ABAQUS, and compared with the upper bound results. These comparisons show a good agreement.
Key words: extrusion; hybrid sheet metal; upper bound method

1 Introduction

Multilayered metal products are used in a variety of industries, such as fabrication of containers and pressure vessels, atomic energy applications and permanent storage of computer data. Hybrid sheet metal consists of two or more sheet metals bonded together and each sheet occupies a distinct position in the component. They are used for economic and structural reasons and production of them by metal forming has become an important subject. The compressive state of stress in extrusion and the possibility of producing metallurgical bonds between the two metals as shown for example in the work by KAZANOWSKI et al [1] in rod extrusion and by MAMALIS et al [2] in tube extrusion, make this process a suitable choice for producing hybrid sheet metals. In this process, alike other metal forming processes, estimation and minimization of the extrusion force are important. The upper bound technique as an analytical method and the finite element method have been widely used for the analysis of the extrusion of bars made of mono-metal and bimetal materials. A number of people have used the upper bound method and FEM to analyze the bimetal extrusion of circular sections with axial symmetry through a variety of die shapes. Finite element methods for the extrusion process are very complicated. To derive accurate results using FEM, the effects of many parameters must be considered. Using FEM for optimum die design is costly and time consuming. After the upper bound model has determined the optimal die shapes, a finite element model has been used to study extrusion through dies with these optimal shapes.

OSAKADA et al [3] described the hydrostatic extrusion of bimetal rods with hard cores through conical dies by the upper bound method. AVITZUR [4] summarized the factors that affect simultaneous flow of layers in extrusion of a bimetal rod through conical dies. TOKUNO and IKEDA [5] verified the deformation in extrusion of composite bars by experimental and upper bound methods. YANG et al [6] studied the axisymmetric extrusion of composite rods through curved dies by experimental and upper bound methods. SLIWA [7] described the plastic zones in the forward extrusion of metal composites by experimental and upper bound methods. CHITKARA and ALEEM [8,9] theoretically studied the mechanics of extrusion of axisymmetric bi-metallic tubes from solid circular bars using fixed mandrel with application of generalized upper bound and slab method analyses. They investigated the effect of different parameters such as extrusion ratio, frictional conditions, and shape of the

Corresponding author: H. HAGHIGHAT; Tel: +98-831-4274530; Fax: +98-831-4274542; E-mail: hhaghighat@razi.ac.ir
DOI: 10.1016/S1003-6326(14)63468-3

dies and that of the mandrels on the extrusion pressures. KANG et al [10] designed the die for hot forward and backward extrusion process of Al-Cu clad composite rod by experimental investigation and FEM simulation. HWANG and HWANG [11] studied the plastic deformation behavior within a conical die during bimetallic rod extrusion by experimental and upper bound methods. HAGHIGHAT and ASGARI [12] proposed a generalized spherical velocity field for bimetal tube extrusion process through dies of any shape.

As mentioned above, most researches were focused on the extrusion of rotation-symmetric bimetal rods or tubes. Regarding the extrusion of non-axisymmetric mono-metal and bimetal extrusion processes, ALTINBALIK and AYER [13] investigated the effect of die inlet and transition geometry on the extrusion loads and material flow for extrusion of clover sections. HAGHIGHAT and AMJADIAN [14] proposed two kinematically admissible velocity fields based on assuming proportional angles and proportional distances from the midline in the deformation zone in upper bound models for plane strain extrusion through arbitrarily curved dies. ENGELHARDT et al [15] investigated experimentally the extrusion of hybrid sheet metals through flat dies.

To overcome deficiencies associated with the flat dies (more redundant work, formation of dead metal zone, etc.), streamlined dies have been used in the extrusion process.

This work is focused on the analysis and finite element simulation of the extrusion of hybrid sheet metals through streamlined dies. An upper bound solution for flow of hybrid sheet metals during extrusion through any possible die shape is developed. Based on this model, for a given process parameter, optimum die shape and the required extrusion force are derived. The FEM simulation on the extrusion of a bimetal sheet composed of a copper sleeve layer and an aluminum core layer is also conducted.

2 Upper bound analysis

The upper bound method is a limit analysis technique that relaxes some of the requirements of an exact solution and in this method, solutions are found by minimizing the total power formulated from a chosen kinematically admissible velocity field. Due to its relaxation of the requirements of an exact solution, upper bound analysis is less computational intensive than finite element method and can quickly evaluate a large number of die shapes.

2.1 Geometric description of deformation zones

Extrusion process of the bimetal sheet through an arbitrary curved die is shown in Fig. 1. An initially sheet, made of two different ductile materials with the mean flow stresses σ_c and σ_s is considered. The subscripts "c" and "s" denote inner material, core, and outer material, sleeve, respectively. The material starts as a hybrid sheet with sleeve thickness $2t_{1o}$ and core thickness $2t_{2o}$ and it extrudes into a product of thicknesses $2t_{2f}$ and $2t_{1f}$ for sleeve and core through a curved die, respectively. Widths of sleeve and core materials are denoted by b_s and b_c, respectively, as shown in Fig. 1.

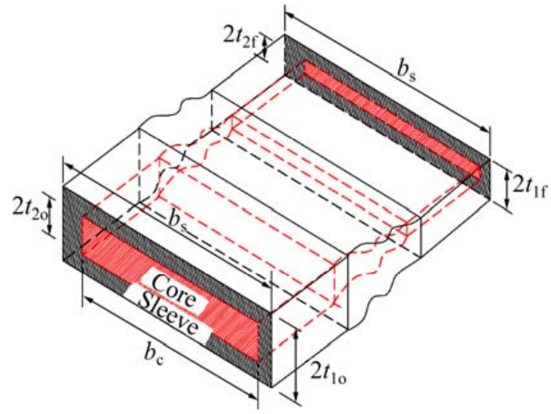

Fig. 1 Extrusion process of hybrid sheet metal through arbitrarily curved die

To analyze the process, the material under deformation is divided into two regions, bimetal region and mono-metal region, and the flow of the material in each region is assumed as plane strain. Figures 2 and 3 show the process parameters in a schematic diagram for mono-metal and bimetal regions, respectively. Taking into account the symmetry of the problem, only half of the section is considered.

To analyze the process by using the upper bound method, the material under deformation in mono-metal region is subdivided into three zones, as shown in Fig. 2. In zones 1 and 3, the material moves rigidly with the velocity V_o and V_f, respectively. The surfaces A_1 and A_2 are located at distances r_o and r_f from the origin O, respectively. The mathematical equations for radial positions of two velocity discontinuity surfaces A_1 and A_2 are given by

$$r_o = \frac{t_{1o}}{\sin\alpha},\ r_f = \frac{t_{1f}}{\sin\alpha} \tag{1}$$

where α is the angle of the line connecting the initial point of the curved die to the final point of the die and

$$\tan\alpha = \frac{t_{1o} - t_{1f}}{L} \tag{2}$$

where L denotes die length.

The die surface, which is labeled as $\psi(r)$ in Figs. 2 and 3, is given in the cylindrical coordinate system (r, θ, z)

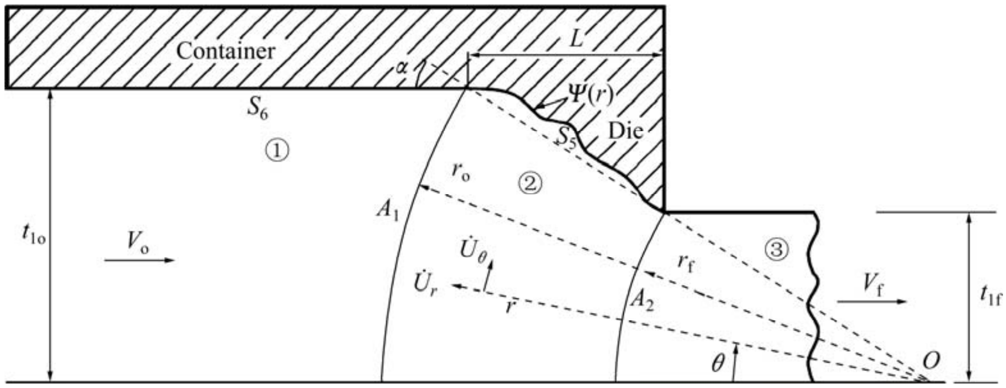

Fig. 2 Schematic diagram of mono-metal sheet extrusion through curved die

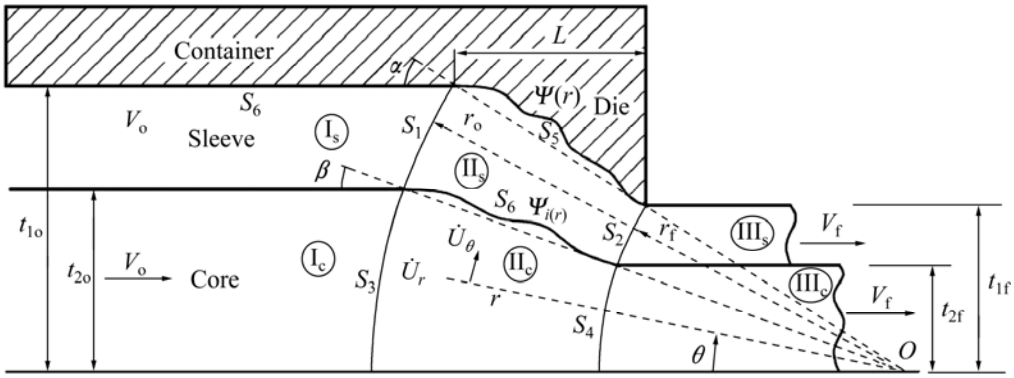

Fig. 3 Schematic diagram of bimetal sheet extrusion through curved die

where $\psi(r)$ is the angular position of the die surface as a function of the radial distance from the origin. The origin of cylindrical coordinate system is located at point O, as shown in Figs. 2 and 3.

Two types of die shapes are examined in the present investigation. The first die shape is wedge shaped die as a linear die profile. This profile has a single constant value, i.e. $\psi(r)=\alpha$. The second die shape is from the work by YANG and HAN [16]. They created a streamlined die shape as a fourth-order polynomial whose slope is parallel to the axis at both entrance and exit. The die profile of YANG and HAN in Cartesian coordinate system, shown in Fig. 4, is given by the following fourth-order polynomial as

$$h(x)=t_{\mathrm{o}}+\frac{1}{L^2}[C_{\mathrm{f}}t_{\mathrm{o}}-3(t_{\mathrm{o}}-t_{\mathrm{f}})]x^2+\frac{1}{L^3}[2(t_{\mathrm{o}}-t_{\mathrm{f}})-2C_{\mathrm{f}}t_{\mathrm{o}}]x^3+\frac{1}{L^4}C_{\mathrm{f}}t_{\mathrm{o}}x^4 \tag{3}$$

Subjected to $h'(0)=h'(L)=0$, $h(0)=t_{\mathrm{o}}$, $h(L)=t_{\mathrm{f}}$ and $C_{\mathrm{f}}=\dfrac{3(1-t_{\mathrm{f}}/t_{\mathrm{o}})(1-2L_{\mathrm{f}}/L)}{1-6L_{\mathrm{f}}/L+6(L_{\mathrm{f}}/L)^2}$

where L_{f}/L is the relative position of the inflection point for the die and can vary from 0 to 1.

Die shape of YANG and HAN was expressed in polar coordinate system, (r, ψ), by Ref. [17] as

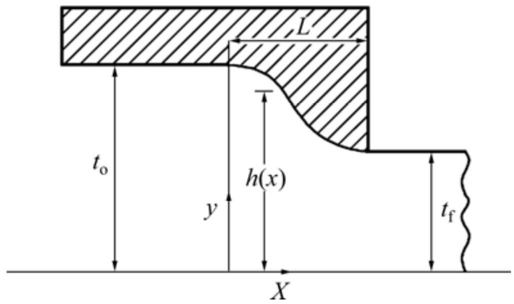

Fig. 4 Sketch of the die shape of YANG and HAN in Cartesian coordinate system

$$\frac{r}{r_{\mathrm{o}}}\frac{\sin\psi}{\sin\alpha}=1+\left(\frac{C_{\mathrm{f}}}{(1-t_{\mathrm{f}}/t_{\mathrm{o}})^2}-\frac{3}{1-t_{\mathrm{f}}/t_{\mathrm{o}}}\right)\left(-\frac{r}{r_{\mathrm{o}}}\frac{\cos\psi}{\cos\alpha}+1\right)^2+\left(\frac{2}{(1-t_{\mathrm{f}}/t_{\mathrm{o}})^2}-\frac{2C_{\mathrm{f}}}{(1-t_{\mathrm{f}}/t_{\mathrm{o}})^3}\right)\left(-\frac{r}{r_{\mathrm{o}}}\frac{\cos\psi}{\cos\alpha}+1\right)^3+\frac{C_{\mathrm{f}}}{(1-t_{\mathrm{f}}/t_{\mathrm{o}})^4}\left(-\frac{r}{r_{\mathrm{o}}}\frac{\cos\psi}{\cos\alpha}+1\right)^4 \tag{4}$$

The material under deformation in bimetal region is subdivided into six zones, as shown in Fig. 3. In zones $\mathrm{I_s}$ and $\mathrm{I_c}$, the incoming sheet is assumed to flow horizontally as rigid body with velocity V_{o}. In zones $\mathrm{III_s}$ and $\mathrm{III_c}$, the extruded sheet is assumed to flow horizontally as rigid body with velocity V_{f}. Zones $\mathrm{II_s}$ and

$\mathrm{II_c}$ are the deformation zones, where the velocity is complex. These zones are surrounded by four velocity discontinuity surfaces S_1, S_2, S_3 and S_4. In addition to these surfaces, there are two frictional surfaces between sleeve and container and die surface and sleeve S_5. The surfaces S_1 and S_3 are located at distance r_o from the origin and the surfaces S_2 and S_4 are located at distance r_f from the origin. The mathematical equations for radial positions of four velocity discontinuity surfaces S_1, S_3 and S_2, S_4 are given by Eq. (2).

The interface surface between the inner and the outer materials is defined by $\psi_i(r)$ which is the angular position of the interface surface as a function of the radial distance from the origin. Angle β, shown in Fig. 3, is given by

$$\sin\beta = \frac{t_{2\mathrm{o}}}{t_{1\mathrm{o}}}\sin\alpha \tag{5}$$

2.2 Velocity fields in deformation zones

The velocity component in the radial direction within the deformation zone, $\dot{U}_r$, can be obtained by assuming volume flow balance. In Fig. 2, assuming proportional distances from the midline in the deformation zone, then the velocity components in the deformation zone can be given by [14]

$$\begin{cases} \dot{U}_r = -V_\mathrm{o}\dfrac{r_\mathrm{o}}{r}\dfrac{\sin\alpha}{\sin\psi}\cos\theta \\ \dot{U}_\theta = -V_\mathrm{o}\, r_\mathrm{o}\dfrac{\sin\alpha}{\sin\psi}\dfrac{\partial\psi}{\partial r}\cot\psi\sin\theta \\ \dot{U}_z = 0 \end{cases} \tag{6}$$

Based on the established velocity field, the strain rate field for deformation zones can be obtained. The strain rates components in cylindrical coordinates are defined as

$$\begin{cases} \dot{\varepsilon}_{rr} = \dfrac{\partial \dot{U}_r}{\partial r} \\ \dot{\varepsilon}_{\theta\theta} = \dfrac{1}{r}\dfrac{\partial \dot{U}_\theta}{\partial\theta} + \dfrac{\dot{U}_r}{r} \\ \dot{\varepsilon}_{zz} = \dfrac{\partial \dot{U}_z}{\partial z} \\ \dot{\varepsilon}_{r\theta} = \dfrac{1}{2}\left(\dfrac{\partial \dot{U}_\theta}{\partial r} + \dfrac{1}{r}\dfrac{\partial \dot{U}_r}{\partial\theta} - \dfrac{\dot{U}_\theta}{r}\right) \\ \dot{\varepsilon}_{\theta z} = \dfrac{1}{2}\left(\dfrac{\partial \dot{U}_\theta}{\partial z} + \dfrac{1}{r}\dfrac{\partial \dot{U}_z}{\partial\theta}\right) \\ \dot{\varepsilon}_{zr} = \dfrac{1}{2}\left(\dfrac{\partial \dot{U}_r}{\partial z} + \dfrac{\partial \dot{U}_z}{\partial r}\right) \end{cases} \tag{7}$$

The strain rate components can be obtained by using group Eqs. (6) and (7) as

$$\begin{cases} \dot{\varepsilon}_{rr} = -\dot{\varepsilon}_{\theta\theta} = V_\mathrm{o}\dfrac{r_\mathrm{o}}{r^2}\dfrac{\sin\alpha}{\sin\psi}\left(1 + r\dfrac{\partial\psi}{\partial r}\cot\psi\right)\cos\theta \\ \dot{\varepsilon}_{r\theta} = \dfrac{1}{2}V_\mathrm{o}\dfrac{r_\mathrm{o}}{r^2}\dfrac{\sin\alpha}{\sin\psi}\left[1 - r^2\cot\psi\dfrac{\partial^2\psi}{\partial r^2} + r^2(1+\cot^2\psi)\cdot\right. \\ \qquad \left.\left(\dfrac{\partial\psi}{\partial r}\right)^2 + \cot^2\psi\left(\dfrac{\partial\psi}{\partial r}\right)^2 + r\cot\psi\dfrac{\partial\psi}{\partial r}\right]\sin\theta \\ \dot{\varepsilon}_{zz} = \dot{\varepsilon}_{\theta z} = \dot{\varepsilon}_{zr} = 0 \end{cases} \tag{8}$$

With the velocity field and the strain rates in the deformation zone, internal power and the power consumed on the shear and frictional surfaces can be given in usual matter.

2.3 Internal power of deformation

The internal power of deformation for a material with mean flow stress of σ_0 in an upper bound model is

$$\dot{W}_i = \frac{2}{\sqrt{3}}\sigma_0\int_V\sqrt{\frac{1}{2}\dot{\varepsilon}_{ij}\dot{\varepsilon}_{ij}}\,\mathrm{d}V \tag{9}$$

Internal powers of zones 1 and 3 are zero and the equation to calculate the internal power of deformation in zone 2, shown in Fig. 2, can be given by

$$\dot{W}_{i2} = \frac{2\sigma_\mathrm{s}}{\sqrt{3}}(b_\mathrm{s} - b_\mathrm{c})\int_{r_\mathrm{f}}^{r_\mathrm{o}}\int_0^{\psi(r)}\sqrt{\frac{1}{2}\dot{\varepsilon}_{rr}^2 + \frac{1}{2}\dot{\varepsilon}_{\theta\theta}^2 + \dot{\varepsilon}_{r\theta}^2}\; r\,\mathrm{d}\theta\,\mathrm{d}r \tag{10}$$

where σ_s is the mean flow stress of sleeve material and is determined by

$$\sigma_\mathrm{s} = \frac{\int_0^\varepsilon \sigma\mathrm{d}\varepsilon}{\varepsilon},\ \ \varepsilon = \ln\frac{t_{1\mathrm{o}}b_\mathrm{s} - t_{2\mathrm{o}}b_\mathrm{c}}{t_{1\mathrm{f}}b_\mathrm{s} - t_{2\mathrm{f}}b_\mathrm{c}} \tag{11}$$

Internal powers of zones $\mathrm{I_s}$, $\mathrm{I_c}$, $\mathrm{III_s}$ and $\mathrm{III_c}$, as shown in Fig. 3, are zero and the equation to calculate the internal power of deformation in zone $\mathrm{II_s}$ is

$$\dot{W}_{i\mathrm{II_s}} = \frac{2\sigma_\mathrm{s}}{\sqrt{3}}b_\mathrm{c}\int_{r_\mathrm{f}}^{r_\mathrm{o}}\int_{\psi_i(r)}^{\psi(r)}\sqrt{\frac{1}{2}\dot{\varepsilon}_{rr}^2 + \frac{1}{2}\dot{\varepsilon}_{\theta\theta}^2 + \dot{\varepsilon}_{r\theta}^2}\; r\mathrm{d}\theta\mathrm{d}r \tag{12}$$

And $\psi_i(r)$ is the angular position of the interface surface as a function of the radial distance from the origin O and is given by

$$\sin\psi_i(r) = \frac{\sin\beta}{\sin\alpha}\sin\psi(r) \tag{13}$$

The general equation to calculate the internal power of deformation in zone $\mathrm{II_c}$ is determined as

$$\dot{W}_{i\mathrm{II_c}} = \frac{2\sigma_\mathrm{c}}{\sqrt{3}}b_\mathrm{c}\int_{r_\mathrm{f}}^{r_\mathrm{o}}\int_0^{\psi_i(r)}\sqrt{\frac{1}{2}\dot{\varepsilon}_{rr}^2 + \frac{1}{2}\dot{\varepsilon}_{\theta\theta}^2 + \dot{\varepsilon}_{r\theta}^2}\; r\mathrm{d}\theta\mathrm{d}r \tag{14}$$

where σ_c is the mean flow stress of core material and is given by

$$\sigma_{\mathrm{c}}=\frac{\int_0^{\varepsilon}\sigma\mathrm{d}\varepsilon}{\varepsilon},\ \varepsilon=\ln\frac{t_{2\mathrm{o}}}{t_{2\mathrm{f}}} \tag{15}$$

2.4 Shear power losses

The equation for the power losses along a shear surface of velocity discontinuity in an upper bound model is

$$\dot{W}_S=\frac{\sigma_0}{\sqrt{3}}\int_S|\Delta v|\mathrm{d}S \tag{16}$$

So, the shear power loss along the velocity discontinuity surface A_1, as shown in Fig. 2, becomes

$$\dot{W}_{SA_1}=\frac{\sigma_{\mathrm{s}}}{\sqrt{3}}V_{\mathrm{o}}\,r_{\mathrm{o}}(b_{\mathrm{s}}-b_{\mathrm{c}})\int_0^{\alpha}(1+r_{\mathrm{o}}\frac{\partial\psi}{\partial r}\Big|_{r=r_{\mathrm{o}}}\cot\alpha)\sin\theta\mathrm{d}\theta \tag{17}$$

And the shear power loss along the surface of velocity discontinuity A_2 becomes

$$\dot{W}_{SA_2}=\frac{\sigma_{\mathrm{s}}}{\sqrt{3}}V_{\mathrm{o}}\,r_{\mathrm{o}}\,(b_{\mathrm{s}}-b_{\mathrm{c}})\int_0^{\alpha}(1+r_{\mathrm{o}}\frac{t_{1\mathrm{o}}}{t_{1\mathrm{f}}}\frac{\partial\psi}{\partial r}\Big|_{r=r_{\mathrm{f}}}\cot\alpha)\cdot\sin\theta\mathrm{d}\theta \tag{18}$$

The shear power loss along the velocity discontinuity surfaces S_1, S_2, S_3 and S_4 can be given by

$$\dot{W}_{S_1}=\frac{\sigma_{\mathrm{s}}}{\sqrt{3}}V_{\mathrm{o}}\,r_{\mathrm{o}}b_{\mathrm{c}}\int_{\beta}^{\alpha}(r_{\mathrm{o}}\frac{\partial\psi}{\partial r}\Big|_{r=r_{\mathrm{o}}}\cot\alpha)\sin\theta\mathrm{d}\theta \tag{19}$$

$$\dot{W}_{S_2}=\frac{\sigma_{\mathrm{s}}}{\sqrt{3}}V_{\mathrm{o}}r_{\mathrm{o}}b_{\mathrm{c}}\int_{\beta}^{\alpha}(1+r_{\mathrm{o}}\frac{t_{\mathrm{o}}}{t_{\mathrm{f}}}\frac{\partial\psi}{\partial r}\Big|_{r=r_{\mathrm{f}}}\cot\alpha)\sin\theta\mathrm{d}\theta \tag{20}$$

$$\dot{W}_{S_3}=\frac{\sigma_{\mathrm{c}}}{\sqrt{3}}V_{\mathrm{o}}\,r_{\mathrm{o}}b_{\mathrm{c}}\int_0^{\beta}(1+r_o\frac{\partial\psi}{\partial r}\Big|_{r=r_{\mathrm{o}}}\cot\alpha)\sin\theta\mathrm{d}\theta \tag{21}$$

$$\dot{W}_{S_4}=\frac{\sigma_{\mathrm{c}}}{\sqrt{3}}V_{\mathrm{o}}r_{\mathrm{o}}b_{\mathrm{c}}\int_0^{\beta}(1+r_{\mathrm{o}}\frac{t_{\mathrm{o}}}{t_{\mathrm{f}}}\frac{\partial\psi}{\partial r}\Big|_{r=r_{\mathrm{f}}}\cot\alpha)\sin\theta\mathrm{d}\theta \tag{22}$$

2.5 Friction power losses and extrusion force

The frictional shear stress is given by $y=m\sigma_0/\sqrt{3}$, where the constant friction factor, m, can take on values from 0 to 1. The general equation for the friction power losses for a surface with a constant friction factor is

$$\dot{W}_{\mathrm{f}}=\frac{\sigma_0}{\sqrt{3}}m\int_S|\Delta v|\mathrm{d}S \tag{23}$$

For die surface

$$\mathrm{d}S=\sqrt{1+(r\frac{\partial\psi}{\partial r})^2}\,\mathrm{d}r \tag{24}$$

and

$$|\Delta v|=\dot{U}_r\cos\eta+\dot{U}_{\theta}\sin\eta|_{\theta=\psi} \tag{25}$$

Angle η is shown in Fig. 5 and it is local angle of the die wall with respect to the local radial velocity component and

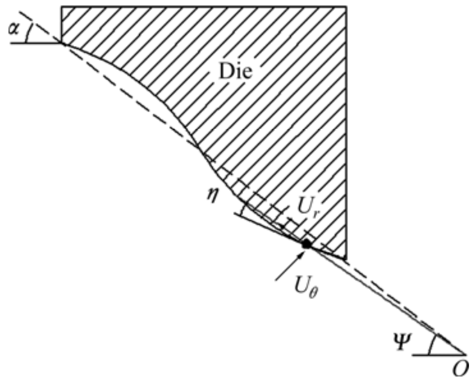

Fig. 5 Angle η between tangent to die profile and radial velocity component at a point on die profile

$$\cos\eta=\frac{1}{\sqrt{1+(r\frac{\partial\psi}{\partial r})^2}},\ \sin\eta=\frac{r\frac{\partial\psi}{\partial r}}{\sqrt{1+(r\frac{\partial\psi}{\partial r})^2}} \tag{26}$$

Placing Eqs. (24)−(26) in Eq. (23), the frictional power losses along die wall, S_5, can be determined as

$$\dot{W}_{\mathrm{f}5}=\frac{\sigma_{\mathrm{s}}}{\sqrt{3}}m_1V_0b_{\mathrm{s}}r_{\mathrm{o}}\int_{r_{\mathrm{f}}}^{r_{\mathrm{o}}}\frac{\sin\alpha}{r\tan\psi}[1+(r\frac{\partial\psi}{\partial r})^2]\mathrm{d}r \tag{27}$$

where m_1 is the constant friction factor between the sleeve and the die.

For the present work, the bonding condition between the core and the sleeve is assumed to be sticky and there is no slippage between core and sleeve materials.

Based on the upper bound model, the total power needed for a bimetal sheet extrusion process can be obtained by summing the internal power and the power dissipated on all frictional and velocity discontinuity surfaces. Then, the total upper bound solution for extrusion force is given by

$$F_{\mathrm{e}}=(\dot{W}_{i2}+\dot{W}_{i\mathrm{II_s}}+\dot{W}_{i\mathrm{II_c}}+\dot{W}_{SA_1}+\dot{W}_{SA_2}+\dot{W}_{S_1}+\dot{W}_{S_2}+\dot{W}_{S_3}+\dot{W}_{S_4}+\dot{W}_{\mathrm{f}_5}/V_0 \tag{28}$$

A MATLAB program has been implemented for the previously derived equations and is used to study the plastic deformation for different die shapes and extrusion conditions. It includes a parameter L, die length that should be optimized. Initial bimetal sheet geometry, friction coefficients, core and sleeve sheet materials properties, reduction in area (RA) and the die shape are input data of the computer program and the computer program calculates the required extrusion force for a given die length.

3 Results and discussion

To make a comparison with the developed model, a bimetal sheet composed of aluminum and copper is used.

The flow stresses for copper and aluminum at room temperature are obtained as [11]

$$\sigma_{Al} = 189.2\,\varepsilon^{0.239}\ \mathrm{MPa} \tag{29}$$

$$\sigma_{Cu} = 335.2\,\varepsilon^{0.113}\ \mathrm{MPa} \tag{30}$$

Friction factor m_1=0.15, m_2=0.9 and reduction in area (RA) 30% are adopted during the analytical solution and the FEM simulation. The configuration of the inner and outer materials is shown in Fig. 6. The extrusion conditions used in the analysis are presented in Table 1.

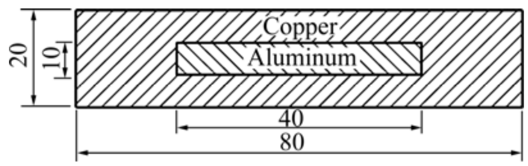

Fig. 6 Cross-section of bimetal sheet before extrusion (Unit: mm)

Table 1 Extrusion conditions used in analysis

Description	Value
t_{1o}, half thickness of sleeve layer in initial sheet/mm	10
t_{2o}, half thickness core layer in initial sheet/mm	5
b_s, widths of sleeve layer/mm	80
t_c, widths of core layer/mm	40
V_o, velocity of initial bimetal sheet/mm	1
m_1, friction factor between sleeve and die	0.15
m_2, friction factor between core and sleeve	0.9
Reduction in area(r_{RA})/%	30, 50 and 65

The developed upper bound solution can be used for the analysis of bimetal sheet extrusion process through dies of any possible shape if the die profile is expressed as equation $\psi(r)$. Two types of die shapes are examined in the present investigation. The first die shape is wedge shaped die as a linear die profile. The second die shape is YANG and HAN die shape as a curved die profile.

In Fig. 7, extrusion forces for the wedge shaped die and the YANG and HAN die shape obtained from the upper bound method are compared with each other. As shown in Fig. 7, the extrusion force of YANG and HAN die shape is lower than that of wedge shaped die. Because this curved die has a smooth transition at the die entrance and exit and shearing in the velocity discontinuity surfaces is zero. At the optimum die length, the extrusion force is minimized.

As shown in Fig. 8, the optimum die length in the case of wedge shaped die is 16 mm and that in the case of YANG and HAN die shape is 15 mm.

The extrusion process is simulated by using the finite element code, ABAQUS. Simulations are done for

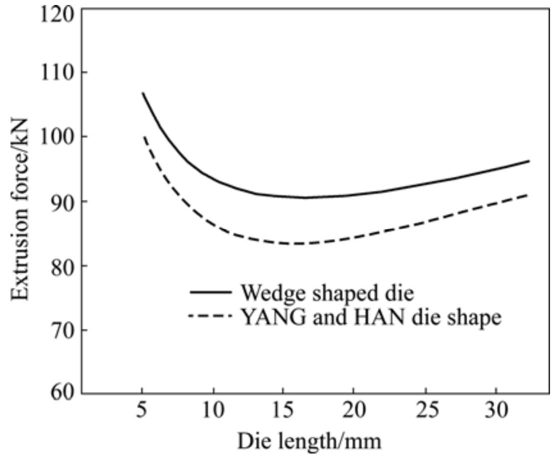

Fig. 7 Comparison of analytical extrusion force values versus die length for wedge shaped die and YANG and HAN die shape for Al−Cu sheet

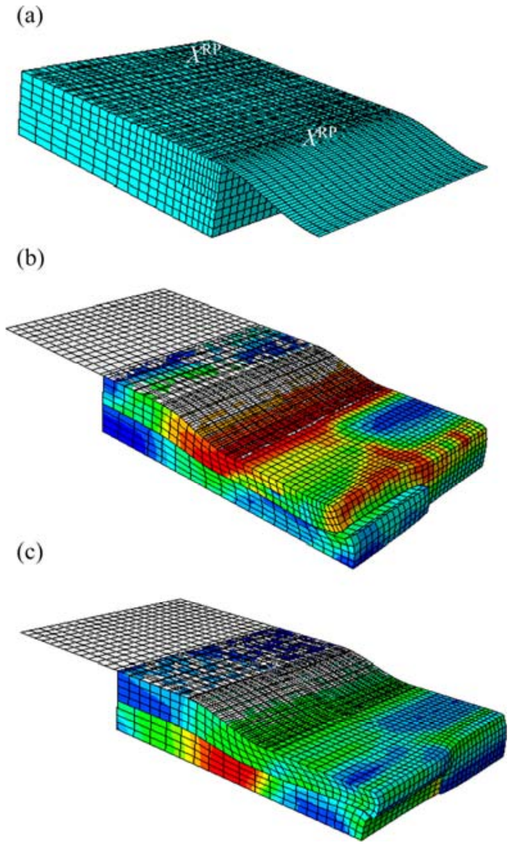

Fig. 8 Finite element mesh and deformed mesh in bimetal sheet extrusion process: (a) Finite element mesh; (b) Deformed mesh for Al−Cu bimetal sheet; (c) Deformed mesh for Cu−Al bimetal sheet

two types of bimetal sheets: aluminum as core, copper as sleeve (Al−Cu) and copper as core, aluminum as sleeve (Cu−Al). Taking into account the symmetries of the process, only one-fourth of the die and the bimetal sheet is considered and the whole model is meshed with C3D8R elements. The punch and the die are modeled as rigid materials. The die model is fixed by applying displacement constraint on its nodes while the punch model is loaded by specifying displacement in the axial direction. Figure 8(a) illustrates the mesh used to analyze the deformation of the optimum YANG and HAN die shape. Deformed models of sleeve and core for two types of sheets (Al−Cu and Cu−Al) are shown in Figs. 8(b) and 8(c), respectively.

The FEM results show that in both types of bimetal sheets, aluminum leaves the deformation zone sooner than copper. Since flow stress of aluminum is lower than that of copper, the former is extruded first. As the applied stress increases to flow stress of copper, simultaneous flow of the two metals continues.

In Figs. 9 and 10, the extrusion force variations during the whole extrusion process obtained from the upper bound solution are compared with the FEM simulation data for the optimum wedge shaped die and optimum YANG and HAN die shape. As shown Figs. 9 and 10, at the early stage of extrusion, unsteady state deformation occurs, and the materials have not yet filled up the cavity of the die completely. Thus, the extrusion force increases as the extrusion process proceeds. After the materials have filled up the cavity of the die completely, the extrusion force decreases gradually. The gradual decrease in the load–displacement curves is due to decreasing the frictional surface area in the container as the punch is advanced.

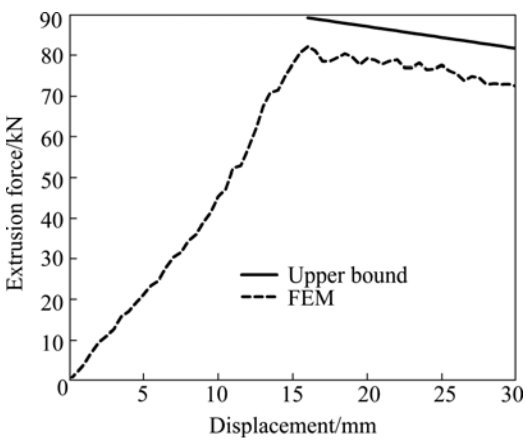

Fig. 9 Comparison of upper bound and FEM extrusion force−displacement curves for optimum wedge shaped for Al−Cu bimetal sheet

As shown in Figs. 9 and 10, the analytically predicted forces are about 13% higher than the FEM results, which is due to the nature of the upper bound theory.

In Fig. 11, the extrusion forces obtained from the upper bound solution are compared with the results obtained by FEM for YANG and HAN die with three different reductions in area, r_{RA}=30%, 50% and 65%. It is obvious that the increase of reduction in area (r_{RA}) increases the extrusion force. The results show good agreement.

The effect of die length on the extrusion force for different values of friction factor is shown in Fig. 12. As

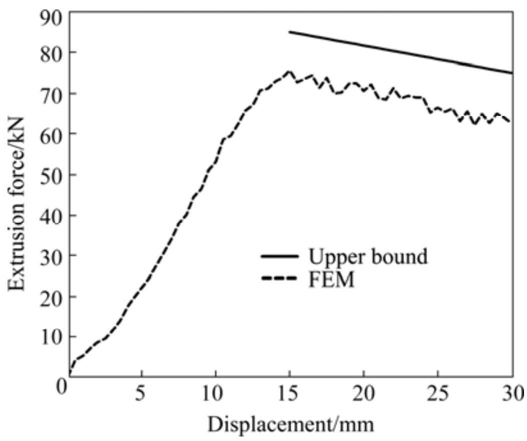

Fig. 10 Comparison of upper bound and FEM extrusion force−displacement curves for optimum YANG and HAN die shape and for Al−Cu bimetal sheet

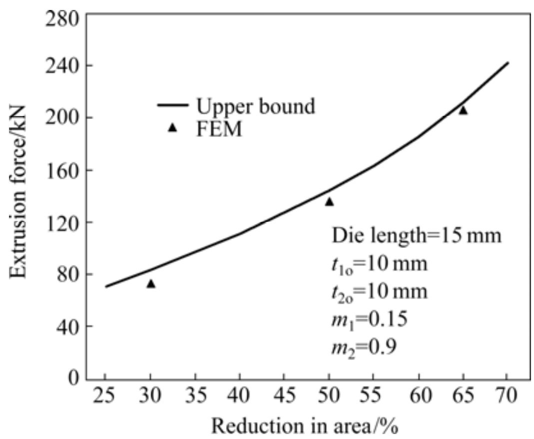

Fig. 11 Comparison of analytical and FEM data for different reductions in area for YANG and HAN die shape

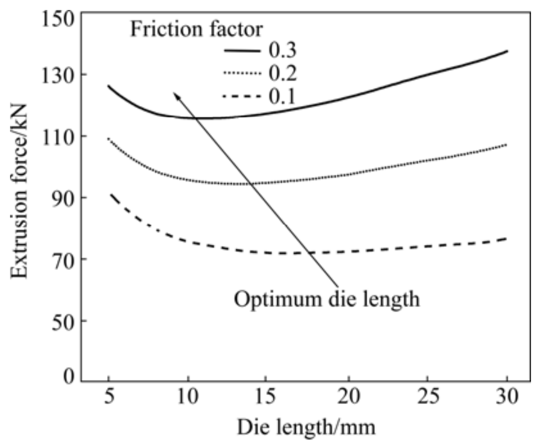

Fig. 12 Optimum die length for different values of friction factor m_1 for YANG and HAN die shape

expected, for a given value of friction factor, the extrusion force is minimized in an optimum die length. It is observed that the optimum die length decreases when shearing friction factor increases. This figure, also, shows that an increase in the friction factor tends to increase the extrusion force.

4 Conclusions

1) By using the developed upper bound model, optimum die lengths for a wedge shaped die and also for Yang and Han die shape were determined.

2) The extrusion force for those two dies have been determined by using the finite element code, ABAQUS, and compared with analytical results. These comparisons show a good agreement.

3) Extrusion pressure of YANG and HAN die shape was lower than wedge shaped die.

References

[1] KAZANOWSKI P, EPLER M E, MISIOLEK W Z. Bi-metal rod extrusion process and product optimization [J]. Materials Science and Engineering A, 2004, 369: 170−180.

[2] MAMALIS A G, PETROSYAN G L, MANOLAKOS D E, PETROSYAN H G. Determination of initial compression stresses when extruding bimetallic tubes with porous internal layer [J]. Journal of Materials Processing Technology, 2006, 172: 277−282.

[3] OSAKADA K, LIMB M, MELLOR P B. Hydrostatic extrusion of composite bars with hard cores [J]. International Journal of Mechanical Sciences, 1973, 15: 291−307.

[4] AVITZUR B. Handbook of metal-forming processes [M]. New York: Wiley, 1983.

[5] TOKUNO H, IKEDA K. Analysis of deformation in extrusion of composite bars [J]. Journal of Materials Processing Technology, 1991, 26: 323−335.

[6] YANG D Y, KIM Y G, LEE C M. An upper-bound solution for axisymmetric extrusion of composite bars through curved dies [J]. International Journal of Mechanical Sciences, 1999, 31: 565−575.

[7] SLIWA R. Plastic zones in the extrusion of metal composites [J]. Journal of Materials Processing Technology, 1997, 67: 29−35.

[8] CHITKARA N R, ALEEM A. Extrusion of axi-symmetric bi-metallic tubes from solid circular bars: Application of a generalized upper bound analysis and some experiments [J]. International Journal of Mechanical Sciences, 2001, 43: 2833−2856.

[9] CHITKARA N R, ALEEM A. Extrusion of axi-symmetric bi-metallic tubes: Some experiments using hollow bars and the application of a generalized slab method of analysis [J]. International Journal of Mechanical Sciences, 2001, 43: 2857−2882.

[10] KANG C G, JUNG Y J, KWON H C. Finite element simulation of die design for hot extrusion process of Al/Cu clad composite and its experimental investigation [J]. Journal of Materials Processing Technology, 2002, 124: 49−56.

[11] HWANG Y M, HWANG T F. An investigation into the plastic deformation behavior within a conical die during composite bar extrusion [J]. Journal of Materials Processing Technology, 2002, 12: 226−233.

[12] HAGHIGHAT H, ASGARI G R. A generalized spherical velocity field for bi-metallic tube extrusion through dies of any shape [J]. International Journal of Mechanical Sciences, 2011, 53: 248−253.

[13] ALTINBALIK T, AYER O. Effect of die inlet geometry on extrusion of clover sections through curved dies: Upper bound analysis and experimental verification [J]. Transactions of Nonferrous Metals Society of China, 2013, 23(4): 1098−1107.

[14] HAGHIGHAT H, AMJADIAN P. A generalized velocity field for plane strain extrusion through arbitrarily curved dies [J]. ASME Journal of Manufacturing Science and Engineering, 2011, 133: 041006.

[15] ENGELHARDT M, GRITTENER N, HAVERKAMP H S, REIMCHE W, BORMANN D, BACH F W. Extrusion of hybrid sheet metals [J]. Journal of Materials Processing Technology, 2012, 212: 1030−1038.

[16] YANG D Y, HAN C H. A new formulation of generalized velocity field for axisymmetric forward extrusion through arbitrarily curved dies [J]. Transactions of the ASME Journal of Engineering for Industry, 1987, 109: 161−168.

[17] GORDON W A, van TYNE C J, MOON Y H. Axisymmetric extrusion through adaptable dies — Part 3: Minimum pressure streamlined die shapes [J]. International Journal of Mechanical Sciences, 2007, 49: 104−115.

复合金属板材曲面模具挤压的上限法分析

H. HAGHIGHAT, H. SHAYESTEH

Mechanical Engineering Department, Razi University, Kermanshah 67149−67346, Iran

摘 要：通过上限法分析了复合金属板材经反复曲面模具的挤压过程。变形材料可以分为双金属区和单金属区 2 个变形区域。每个区域材料的流变状态都设为平面应变状态。得到内能，剪切能和摩擦能的表达式，并应用到上限模型中。确定了铜包覆铝复合材料采用楔形模具和流线曲面模具的挤压力。通过有限元软件 ABAQUS 模拟得到 2 种模具的相应结果，并与上限法模型进行对比，比较结果表明，两者具有很好的一致性。

关键词：挤压；复合金属板材；上限法

(Edited by Yun-bin HE)